NASA CR-54974
4531-6005-R0000

FINAL REPORT

AN ANALYTICAL STUDY OF LIQUID OUTFLOW FROM CYLINDRICAL TANKS DURING WEIGHTLESSNESS

by

Leslie R. Koval and Pravin G. Bhuta

prepared for

NATIONAL AERONAUTICS AND SPACE ADMINISTRATION

June 1, 1966

CONTRACT NAS 3-7931

Technical Management

NASA Lewis Research Center
Cleveland, Ohio

Spacecraft Technology Division
Donald A. Petrash
Lynn S. Grubb

TRW SYSTEMS GROUP
One Space Park
Redondo Beach, California

CONTENTS

AN ANALYTICAL STUDY OF LIQUID OUTFLOW FROM CYLINDRICAL TANKS DURING WEIGHTLESSNESS

by

Leslie R. Koval and Pravin G. Bhuta

ABSTRACT

In this investigation, a theoretical solution is given for the configuration of the liquid-vapor interface during liquid outflow from a cylindrical, flat-bottomed tank under conditions of weightlessness. The study, which is intended to complement and support the experimental drop tower program at NASA LeRC, is an attempt to obtain an engineering solution to a physical problem which is quite complex because of the effects of viscosity and non-linearities associated with the motion of the interface. The linearized solution presented assumes inviscid, incompressible, and irrotational flow. It is found that the interface can be expected to oscillate during outflow, and that the Weber number is the appropriate scaling parameter (for draining during a state of complete weightlessness).

AN ANALYTICAL STUDY OF LIQUID OUTFLOW FROM CYLINDRICAL TANKS DURING WEIGHTLESSNESS

By Leslie R. Koval and Pravin G. Bhuta
TRW Systems Group

SUMMARY

In this investigation a theoretical solution is given for the liquid-vapor interface configuration during liquid outflow from a cylindrical, flat-bottomed tank under conditions of weightlessness. The study is intended to complement and support the experimental drop tower program at NASA LeRC. The actual problem is quite complex due to the effects of viscosity and nonlinearities associated with the dynamics of the liquid-vapor interface. Because of the need for engineering design information, a linearized solution is presented which assumes inviscid, incompressible, and irrotational flow.

It is found that the interface can be expected to oscillate during outflow, and that the Weber number is an appropriate scaling parameter.* The results of this study indicate that to scale the phenomenon one must preserve the values of Weber number, the ratio of the fill depth to the tank radius, and the ratio of the outlet and tank radii. For small Weber numbers and large fill depths, several oscillations of the liquid-vapor interface take place and this can affect the vapor ingestion time and the amount of liquid remaining in the tank when it occurs. For larger Weber numbers and smaller fill depths, the interface oscillations are unimportant in regard to the draining process. Several numerical calculations have been made.

An attempt has been made to assess the importance of viscosity in different size tanks by examining the ratio of the thickness of the boundary layer to the tank radius. It is found that viscous effects could be important in small diameter tanks.

1. INTRODUCTION

With the progress in space exploration, there will soon arise the need to transfer propellants and other liquids during orbit or coast phases in space. The transfer of liquids may be required from an orbital tanker to a spacecraft, or within a space vehicle such as a manned space station. The present investigation was undertaken to complement the experimental work being conducted at NASA Lewis Research Center and concerns the draining of a liquid under zero gravity conditions. However, the formulations given are sufficiently general to enable one to consider the effects of rigid-body tank motions or the low acceleration levels which may be present during drainage. The analysis is also capable of treating the filling of tanks, although the numerical results given concern only the drainage problem.

* If draining takes place in low-g, the Bond number also enters as a parameter.

The experimental work currently conducted in drop tower tests is limited to the use of small tanks because of the limited zero-g test time available. Hence, one of the objectives of the present analysis was to investigate the effects of tank size and liquid properties on the draining phenomenon with a view to developing scaling laws.

In this investigation, a theoretical solution is given for the propellant outflow from a cylindrical tank with a flat bottom during conditions of weightlessness. The actual physical problem is quite complex because of the effects of viscosity and the nonlinearities. This investigation is an attempt to formulate a simplified mathematical model by assuming the liquid to be inviscid and by considering the linearized problem. Rather than to attempt to solve the complicated nonlinear problem, the purpose of this investigation is to obtain the linearized solution and to compare the theoretical results with those from experiments. If the results of the comparison indicate a need, a nonlinear solution will be suggested to obtain further insight into the draining phenomenon.

The limitations of the linearized solution are recognized at the outset. It is important to emphasize that an engineering solution is sought to provide guidance in the design of space systems. Such a procedure is frequently employed in technology where a linearized solution is used as a first approximation to a nonlinear problem. For example, if one is interested in the vibrations of a simple pendulum for large amplitudes, the problem is nonlinear and its solution is somewhat involved. However, the linearized problem is quite simple and does provide a good engineering estimate of the oscillation frequency for amplitudes as large as 30 degrees* which are certainly beyond the limits for which the linear solution is rigorously valid. Similar situations also arise in other problems in mechanics.

Although the linear solution would not be valid near vapor ingestion, it is used to study the theoretical trends predicted by extrapolating the linearized solution in this regime in an attempt to obtain engineering information needed for the design of future systems.

It should be noted here that the problem of draining of liquid from a tank in a weightless environment differs from other zero-g sloshing problems in that there is no stable equilibrium shape of the liquid-vapor interface about which one can perturb as is done in sloshing problems.

2. MATHEMATICAL FORMULATION

Although the basic mathematical model has been previously formulated in Reference 1, it is given here for the purpose of making this report self-contained. Attention is restricted to axisymmetric draining in a circular tank with a flat bottom having a drain hole in the center. The analysis of Reference 1 is extended to the case of a parabolic velocity distribution at the tank outlet and an initial quiescent hemispherical liquid-vapor interface has been assumed.

*The linearized solution agrees with the nonlinear solution to within 7-1/2 percent at 30-degree amplitude.

Consider the cylindrical coordinate system (R, θ, Z) attached to the bottom of the tank as shown in Figure 1. The mean free surface height is denoted by H(t). The radii of the outlet and the tank are denoted by d and a, respectively. The liquid is assumed to be inviscid and incompressible and the flow irrotational. Hence, within the liquid a velocity potential ϕ exists and satisfies Laplace's equation

$$\frac{\partial^2 \phi}{\partial R^2} + \frac{1}{R}\frac{\partial \phi}{\partial R} + \frac{\partial^2 \phi}{\partial Z^2} = 0 \qquad (1)$$

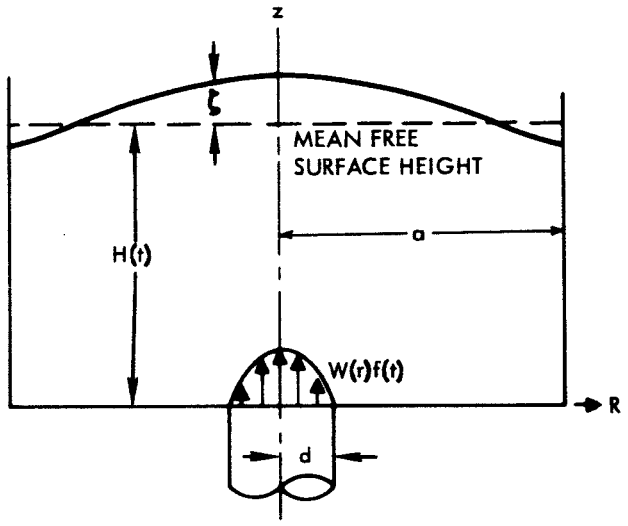

FIGURE 1. —Geometry of the Problem

The components of the liquid velocity relative to the tank in the radial and axial directions are obtained from

$$u = \frac{\partial \phi}{\partial R}, \quad w = \frac{\partial \phi}{\partial Z} \qquad (2)$$

The requirement that the normal component of the velocity vanishes at the wall gives

$$\left.\frac{\partial \phi}{\partial R}\right|_{R = a} = 0 \qquad (3)$$

The boundary condition to be satisfied at the bottom of the tank is

$$\left.\frac{\partial \phi}{\partial Z}\right|_{Z=0} = \begin{cases} W(R)f(t), & 0 \le R \le d \\ 0, & d < R \le a \end{cases} \tag{4}$$

The kinematic free-surface condition, which requires that a particle on the free surface moves with the velocity of the free surface in the vertical direction (Reference 2), yields

$$\dot{H} + \frac{\partial \zeta}{\partial t} + u \left.\frac{\partial \zeta}{\partial R}\right|_{Z=H+\zeta} = w \tag{5}$$

where ζ is the free-surface wave height measured from the mean free-surface height $H(t)$, t is the time, and the components of velocity (u, w) are evaluated on the free surface. The dynamic condition to be satisfied on the free surface is obtained from the integral of the equations of motion, viz.,

$$\left\{\frac{p}{\rho} + \frac{\partial \phi}{\partial t} + \frac{1}{2}(u^2 + w^2) + gZ\right\}_{Z=H+\zeta} = F(t) \tag{6}$$

where p is the pressure, and $F(t)$ is an arbitrary function of time. If surface-tension effects are included, the pressure on the free surface is related to the surface-tension forces in the linear theory by

$$p = -\sigma \nabla^2 \zeta = -\sigma \left(\frac{\partial^2 \zeta}{\partial R^2} + \frac{1}{R}\frac{\partial \zeta}{\partial R}\right) \tag{7}$$

where σ is the surface tension force per unit length. On the free surface

$$Z_{FS}(R, t) = H(t) + \zeta(R, t) \tag{8}$$

and the kinematic free-surface condition, Equation (5), when linearized under the assumption that slopes of the free-surface waves and the radial component of the velocity on the free surface are small, takes the form

$$\left.\frac{\partial \phi}{\partial Z}\right|_{Z=H} = \dot{H} + \frac{\partial \zeta}{\partial t} \tag{9}$$

where the dot denotes differentiation with respect to time and $\partial\phi/\partial Z$ is evaluated on the mean free surface height, H(t). Substituting Equations (2) and (5) into Equation (6) gives

$$\left\{ \frac{p}{\rho} + \frac{\partial\phi}{\partial t} + \frac{1}{2}\left[\left(\frac{\partial\phi}{\partial R}\right)^2 + \left(\dot{H} + \frac{\partial\zeta}{\partial t} + \frac{\partial\phi}{\partial R}\frac{\partial\zeta}{\partial R} \right)^2 \right] + gZ \right\}_{Z=H+\zeta} = F(t) \qquad (10)$$

Neglecting squares of $\partial\phi/\partial R$, $\partial\zeta/\partial t$, etc., in Equation (10), substituting from Equation (7), and rearranging gives

$$\left(\frac{\partial\phi}{\partial t}\right)_{Z=H} + \dot{H}\frac{\partial\zeta}{\partial t} - \frac{\sigma}{\rho}\nabla^2\zeta + g\zeta = F(t) - \frac{1}{2}\dot{H}^2(t) - gH(t) \qquad (11)$$

where $\partial\phi/\partial t$ is evaluated at $z = H$ due to the linearization. Since the right-hand member of Equation (11) is a function of time alone, it may be set equal to zero by incorporating it into the definition of ϕ. Hence, the dynamic free-surface condition of Equation (11) becomes

$$\left(\frac{\partial\phi}{\partial t}\right)_{Z=H} + \dot{H}\frac{\partial\zeta}{\partial t} - \frac{\sigma}{\rho}\nabla^2\zeta + g\zeta = 0 \qquad (12)$$

Equations (1), (3), (4), (9), and (12) define the boundary-value problem to be solved. The initial-value problem is formulated in a later section.

3. SOLUTION OF THE BOUNDARY VALUE PROBLEM

In this section the differential equations governing the time variation of the free-surface motion and the velocity potential are derived for the axisymmetric problem under consideration. The derivation of the equations will involve Bessel functions of the first kind and orders 1, 2, 3 and an expansion into a Fourier-Bessel series.

For the axisymmetric case a solution of Equation (1) which is regular at the origin may be written as

$$\phi_n = J_o(k_n R)\left[\dot{A}_n(t)\cosh k_n Z + \dot{B}_n(t)\sinh k_n Z \right], \quad k_n \neq 0 \qquad (13)$$

where $\dot{A}_n(t)$ and $\dot{B}_n(t)$ are undetermined functions of time, k_n is a constant, and J_o is the Bessel function of the first kind and order zero. When $k_n = 0$, a solution of Equation (1) which is regular at R = 0 is

$$\phi_o = \dot{A}_o(t) + \dot{B}_o(t)\, Z \tag{14}$$

where $\dot{A}_o(t)$ and $\dot{B}_o(t)$ are to be determined. The total potential ϕ is given by summation of ϕ_o and ϕ_n over n from one to infinity. Application of the boundary condition of Equation (3) to Equation (13) yields

$$J_1(k_n a) = 0 \tag{15}$$

which determines the values of k_n. It should be noted that $k_n = 0$ is a solution of Equation (15). Equation (14) identically satisfies the condition of Equation (3). Let the free-surface wave height ζ be given by

$$\zeta(R, t) = \sum_{n=1}^{\infty} C_n(t)\, J_o(k_n R) \tag{16}$$

To make the problem more realistic, the outlet velocity is assumed to have a parabolic variation at the tank outlet.† Accordingly, the boundary condition of Equation (4) takes the form

$$\left.\frac{\partial \phi}{\partial Z}\right|_{Z=0} = \begin{cases} -2\, W_o \left[1 - \dfrac{R^2}{d^2}\right] f(t), & 0 \le R \le d \\ 0, & d \le R \le a \end{cases} \tag{17}$$

where W_o is the average outlet velocity. To satisfy the boundary condition of Equation (17) we expand the parabolic velocity distribution in a Fourier-Bessel series*

$$\left.\frac{\partial \phi}{\partial Z}\right|_{Z=0} = \frac{W_o d^2}{a^2} f(t) + 8 W_o f(t) \sum_{n=1}^{\infty} \frac{J_2(k_n d) J_o(k_n R)}{(k_n a)^2 \left[J_o(k_n a)\right]^2} \tag{18}$$

where

$$J_2(k_n d) = \frac{2}{k_n d} J_1(k_n d) - J_o(k_n d) \tag{18a}$$

† Such an assumption improves the convergence process also because the discontinuity now occurs in the derivatives of the function rather than in the function itself.

* Details are given in Appendix A.

From Equations (13), (14), and (18),

$$\dot{B}_o(t) = -\frac{W_o d^2}{a^2} f(t) \tag{19}$$

and

$$\dot{B}_n(t) = -\frac{8W_o J_2(k_n d) f(t)}{k_n^3 a^2 \left[J_o(k_n a)\right]^2} \tag{20}$$

Use of the kinematic free-surface condition of Equation (9) yields

$$\dot{B}_o(t) = \dot{H} \tag{21}$$

and

$$\dot{A}_n k_n \sinh k_n H + \dot{B}_n k_n \cosh k_n H = \dot{C}_n \tag{22}$$

Equations (19) and (21) show that the continuity requirement relating the rate of change of mean free-surface height, H(t), to the outlet velocity is satisfied. The dynamic free-surface condition of Equation (12) requires

$$\ddot{A}_o = -\ddot{B}_o H \tag{23}$$

and

$$\ddot{A}_n \cosh k_n H + \ddot{B}_n \sinh k_n H + \ddot{H} C_n + \left[\frac{\sigma}{\rho} k_n^2 + g\right] C_n = 0 \tag{24}$$

Eliminating A_n in Equations (22) and (24) results in an uncoupled equation for C_n, viz.,

$$\ddot{C}_n - \frac{2k_n \dot{H} \dot{C}_n}{\sinh 2k_n H} + \left\{\frac{\sigma}{\rho} k_n^3 + g k_n\right\} \tanh k_n H C_n = \frac{k_n \ddot{B}_n}{\cosh k_n H} - \frac{\dot{B}_n k_n^2 \dot{H}}{\sinh k_n H} \tag{25}$$

By the use of Equations (19) to (21), Equation (25) may be written as

$$\ddot{C}_n - \frac{2k_n \dot{H} \dot{C}_n}{\sinh 2k_n H} + \left\{\frac{\sigma}{\rho} k_n^3 + g k_n\right\} \tanh k_n H C_n = \frac{8J_2(k_n d)\ddot{H}}{k_n^2 d^2 \left[J_o(k_n a)\right]^2 \cosh k_n H} - \frac{8J_2(k_n d)\dot{H}^2}{k_n d^2 \sinh k_n H \left[J_o^2(k_n a)\right]^2} \tag{26}$$

To evaluate the free-surface distortion ζ one needs to solve Equation (26) for given initial conditions, for various values of k_n given by Equation (15), and for the prescribed outlet velocity. One then uses Equation (16) to sum the modes. From Equations (19) and (21),

$$\dot{H}(t) = -\frac{W_o d^2}{a^2} f(t) \tag{27}$$

In the particular problem under consideration, the outflow rate is taken as constant, so that Equation (27) takes the form

$$\dot{H}(t) = -\frac{W_o d^2}{a^2} \tag{28}$$

and the second derivative term in the right-hand side of Equation (26) vanishes. In addition, the environment in the problem under consideration is weightless so that $g = 0$.

4. THE INITIAL VALUE PROBLEM

It was shown in Reference 1 that specifying the initial displacement and velocity of the free surface and the liquid outflow rate is sufficient to permit the computation of the subsequent behavior of the free surface. For the particular problem under consideration, the environment is one of weightlessness so that the free surface may initially be approximated as a hemisphere and is at rest when the tank begins to drain. Thus, the initial values for C_n are

$$C_n(0) = C_{no} \tag{29}$$

$$\dot{C}_n(0) = 0$$

where C_{no} is the Fourier-Bessel coefficient in the expansion of the initial hemispherical configuration in a series of $J_o(k_n R)$. The details of the expansion are given in Appendix B, and the result is

$$C_n(0) = -\frac{2a\sqrt{2}\,\Gamma\left(\frac{3}{2}\right) J_{3/2}(k_n a)}{(k_n a)^{3/2}\left[J_o(k_n a)\right]^2} \tag{30}$$

where $\Gamma(3/2)$ is the Gamma function of argument 3/2 and $J_{3/2}(k_n a)$ is the Bessel function of the first kind of order 3/2.

The expression for H(t) is[†]

$$H(t) = H_o - At$$

where $A = W_o d^2/a^2$

5. NON-DIMENSIONALIZATION OF EQUATIONS

For purposes of computation and presentation of the results, it is convenient to non-dimensionalize the equations. Accordingly, we define the non-dimensional quantities:

$$\left.\begin{aligned}
\tau &= t\sqrt{\frac{\sigma}{\rho a^3}} \\
r &= \frac{R}{a} \\
\delta &= \frac{d}{a} \\
\gamma_n &= k_n a \\
h(\tau) &= h_o - \alpha\tau \\
h_o &= \frac{H_o}{a} \\
\alpha &= A\sqrt{\frac{\rho a}{\sigma}} \\
B_o &= \text{Bond No.} = \frac{\rho g a^2}{\sigma} \\
\xi_n &= \frac{C_n}{a} \\
z &= Z/a
\end{aligned}\right\} \qquad (32)$$

[†]Constant outflow rate is assumed.

Introducing Equation (32) into Equations (8), (16), (26), (29), (30) the key equations become

$$Z_{FS} = h(\tau) + \sum_{n=1}^{\infty} \xi_n(\tau)\, J_o(\gamma_n r) \tag{33}$$

$$\xi_n(0) = -\frac{2\sqrt{2}\,\Gamma(3/2) J_{3/2}(\gamma_n)}{\gamma_n^{3/2} J_o^2(\gamma_n)} \tag{34}$$

$$\xi_n'(0) = 0 \tag{35}$$

and

$$\xi_n'' - \left\{\frac{2\gamma_n h'}{\sinh(2\gamma_n h)}\right\} \xi_n' + \left\{(\gamma_n^3 + B_o\gamma_n)\tanh \gamma_n h\right\} \xi_n$$

$$= -\frac{8J_2(\gamma_n\delta)\left[h'\right]^2}{\gamma_n\delta^2 \sinh \gamma_n h\, J_o^2(\gamma_n)} + \frac{8J_2(\gamma_n\delta)h''}{\gamma_n^2\delta^2 J_o^2(\gamma_n) \cosh \gamma_n h} \tag{36}$$

where Z_{FS} is the height of the free surface at location r at time τ, and primes denote differentiation with respect to τ. In the case of a constant outflow rate indicated in Equation (32), the second term in the right hand side of Equation (36) is zero. Also,

$$J_2(\gamma_n\delta) = \frac{2}{\gamma_n\delta} J_1(\gamma_n\delta) - J_o(\gamma_n\delta) \tag{37}$$

Equation (36) will be integrated numerically, subject to the initial conditions given in Equations (34) and (35). Then the summation indicated in Equation (33) gives the free surface shape. The result gives the height of the free surface above the bottom of the container at any time τ. In the numerical computations, the series is truncated at N terms.

6. VAPOR INGESTION

Of prime concern in this draining study is the determination of the time when vapor ingestion occurs and the amount of propellant remaining in the tank when the vapor blowthrough takes place. Vapor ingestion will occur when the liquid free surface intersects with the edge of the outlet, as pictured in Figure

2. Once vapor injestion has occurred, the outflow will be a two phase mixture of liquid and pressurant or ullage gas.

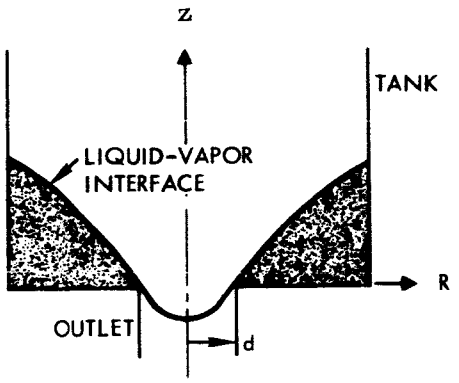

FIGURE 2. —Free Surface Configuration at Vapor Ingestion

Vapor ingestion will occur at time $t = T$ when

$$Z_{FS}(d, T) = (H_o - AT) + \sum_{n=1}^{\infty} C_n(T) J_o(k_n d) = 0 \tag{38}$$

The volume of propellant remaining in the container at this time is

$$V_{BT} = 2\pi \int_d^a Z_{FS}(R, T)\, R\, dR \tag{39}$$

or

$$V_{BT} = 2\pi(H_o - AT)\frac{a^2 - d^2}{2} + 2\pi \sum_{n=1}^{\infty} C_n(T) \int_d^a J_o(k_n R) R\, dR \tag{40}$$

which integrates to

$$V_{BT} = \pi a^3 \left\{ \frac{H_o - AT}{a} \left(1 - \frac{d^2}{a^2}\right) - 2 \sum_{n=1}^{\infty} \frac{(d/a)\frac{c_n(T)}{a}}{k_n a} J_1(k_n d) \right\} \tag{41}$$

The percent volume of propellant remaining at blowthrough is thus

$$\%VRBT = 100\left\{\left(\frac{h_o - \alpha\tau^*}{h_o}\right)(1 - \delta^2) - \frac{2}{h_o}\sum_{n=1}^{\infty}\frac{\delta\,\xi_n(\tau^*)}{\gamma_n}J_1(\gamma_n\delta)\right\} \qquad (42)$$

where the result has been cast into non-dimensional form, and τ^* is the value of τ when vapor ingestion occurs and is determined from

$$0 = (h_o - \alpha\tau^*) + \sum_{n=1}^{\infty}\xi_n(\tau^*)\,J_o(\gamma_n\delta) \qquad (43)$$

In the computations, $Z_{FS}(\delta, \tau)$ is computed for different values of τ until it decreases to zero. This determines τ^*, and %VRBT is then computed.

7. NUMERICAL CALCULATIONS

In this study, numerical calculations have been made for the following cases:

Group I

$We = 0.2, 0.4, 1, 3, 10, 100$

$\frac{\sigma}{\rho} = 30\ cm^3/sec^2$, $\delta = 0.10$

$h_o = 3, 6$

Group II

$We = 0.2, 1, 3, 10$

$\frac{\sigma}{\rho} = 30\ cm^3/sec^2$, $h_o = 3$

$\delta = 0.05, 0.20$

Group III

$We = 0.2, 1, 3, 10$

$\frac{\sigma}{\rho} = 10, 70\ cm^3/sec^2$

$\delta = 0.10$, $h_o = 3$

Additional calculations were made for the following larger initial depths:

We	h_o
0.2	2, 4
1	9
3	18
10	2, 4, 5, 21
100	21

for $\sigma/\rho = 30\ cm^3/sec^2$ and $\delta = 0.10$

The quantity We denotes the Weber number[†] and is given by

$$We = \frac{\rho A^2 a}{4\sigma} \tag{44}$$

This is directly related to the non-dimensional draining rate parameter, α, by

$$We = \frac{1}{4}\left(A\sqrt{\frac{\rho a}{\sigma}}\right)^2 = \frac{\alpha^2}{4} \tag{45}$$

Thus, larger values of We correspond to faster non-dimensional draining rates. Further, because of the non-dimensionalization employed, the non-dimensional times τ^* at which vapor ingestion occurs and the percentage of propellant remaining in the tank are independent of the radius of the tank.[††] Thus, for given values of δ and h_o, all runs at the same value of We are identical.

It should be remarked at this point that the free surface was assumed to be initially quiescent and hemispherical in shape. In an actual space vehicle, there will be many small disturbances to which the free surface will be subjected so that it will very likely have an initial velocity and it may not be perfectly hemispherical when the draining process is started. This will, of course, affect the draining time as well as the volume of liquid remaining in the tank at blow-through. However, results for any given set of initial conditions can easily

---

[†] This definition of Weber number is used to represent the results of this study in a manner consistent with the presentation of the experimental results to be reported by NASA Lewis Research Center.

[††] This can be seen by inspection of Equation (36). The time in seconds will, of course, be affected by the value of tank radius.

be obtained by making the appropriate changes in the initial conditions of the program.

In all cases (except where noted), calculations were made for a liquid in a state of complete weightlessness ($B_o = 0$) and the series in Equation (38) was truncated at 6 terms.

8. SCALING LAWS

Based on the non-dimensionalization employed, scaling laws for the draining problem can now be formulated. Two draining problems will be completely identical if the following quantities for the model and the prototype are maintained.

$$We = \frac{\rho A^2 a}{4\sigma}, \quad \delta = \frac{d}{a}, \tag{46}$$

$$h_o = \frac{H_o}{a}, \quad \tau = t\sqrt{\frac{\sigma}{\rho a^3}}$$

If, further, the environment is not one of weightlessness, then the Bond number

$$B_o = \frac{\rho g a^2}{\sigma} \tag{47}$$

must also be preserved.

9. NUMERICAL RESULTS

The quantities of interest in this study have been the displacement of the centerline of the free surface, the time to vapor ingestion and the percent of the original liquid volume remaining in the tank when "blowthrough", or vapor ingestion, occurs.

Figures 3 through 8 represent the time history of the vertical position of the free surface centerline as the tank drains. The six values of We represent six different values of non-dimensional draining rates, with the larger values corresponding to faster rates. The initial fill depth in each case has been chosen such that the draining time corresponds to more than three cycles of the fundamental sloshing motion. For this reason, there are oscillations about the instantaneous position of the mean free level. If the draining time is fast and the initial fill level is small, there will be less than one cycle of sloshing motion, as is illustrated in Figure 9. The time at which vapor ingestion

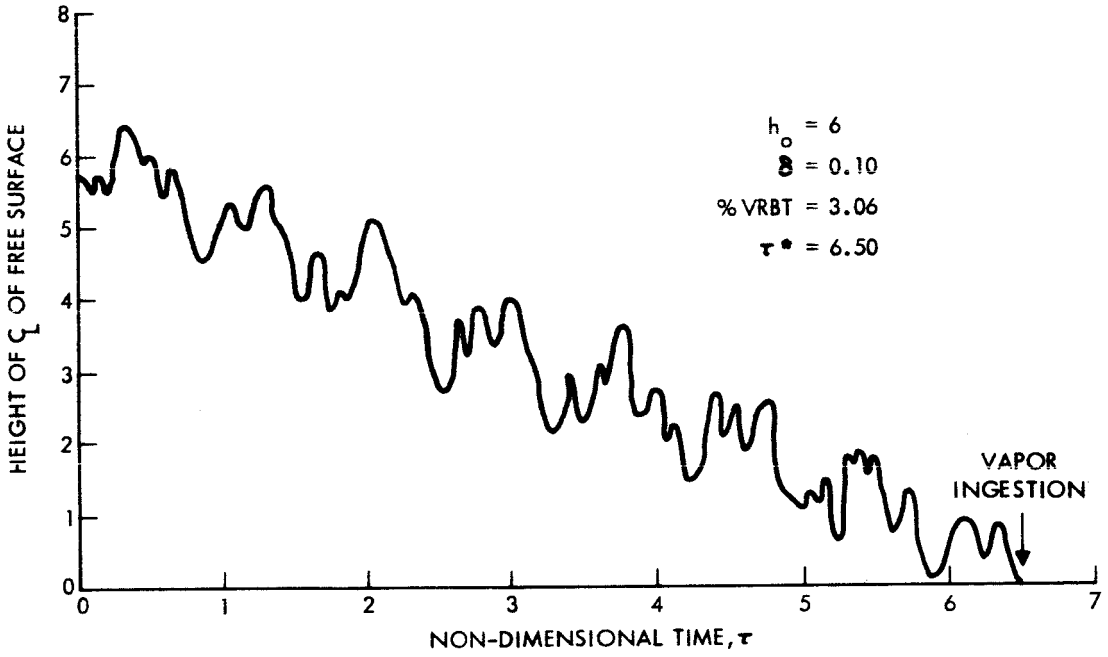

FIGURE 3. — Time-History of Position of Centerline of Liquid-Vapor Interface During Draining for We = 0.2

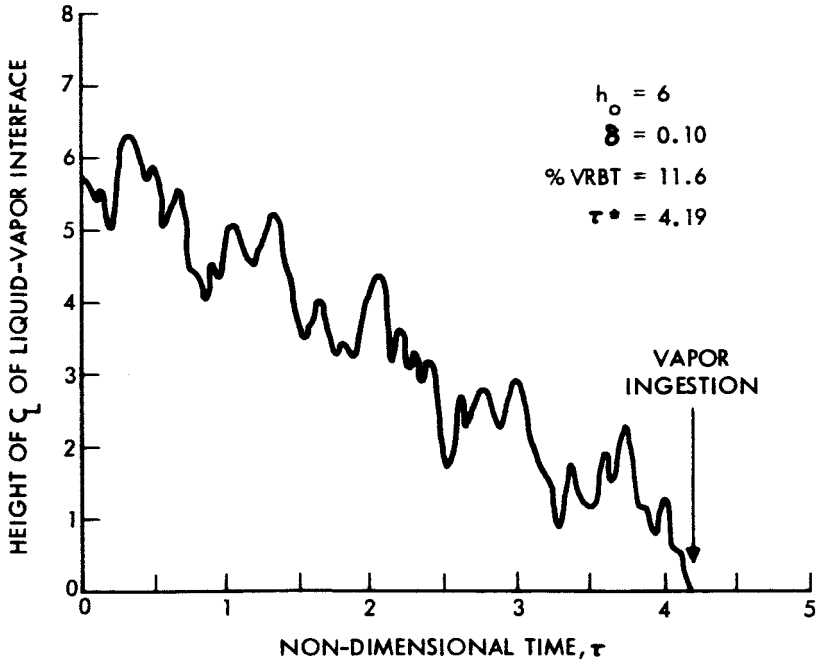

FIGURE 4. — Time-History of Position of Centerline of Liquid-Vapor Interface during Draining at We = 0.4

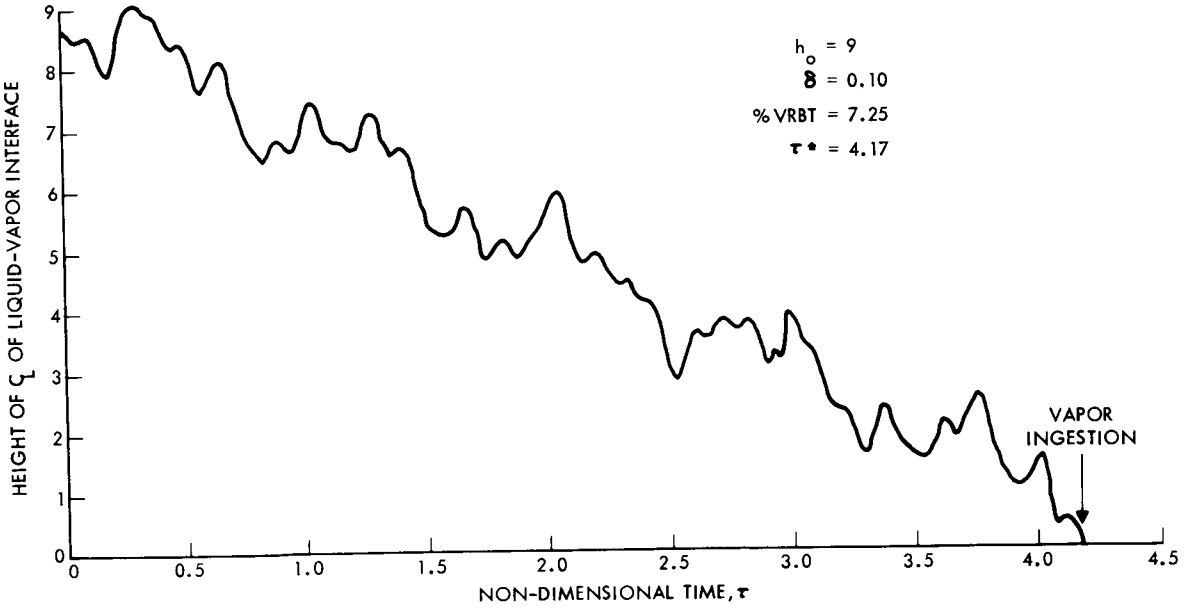

FIGURE 5. —Time-History of Position of Centerline of Liquid-Vapor Interface During Draining at We = 1.0

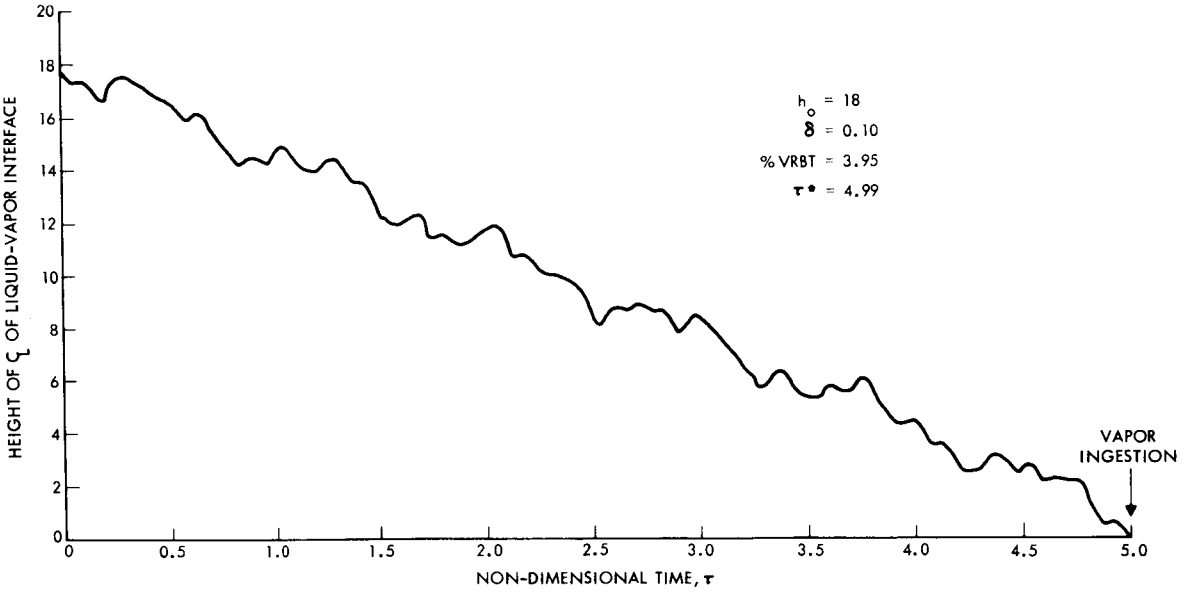

FIGURE 6. —Time-History of Position of Centerline of Liquid-Vapor Interface During Draining at We = 3

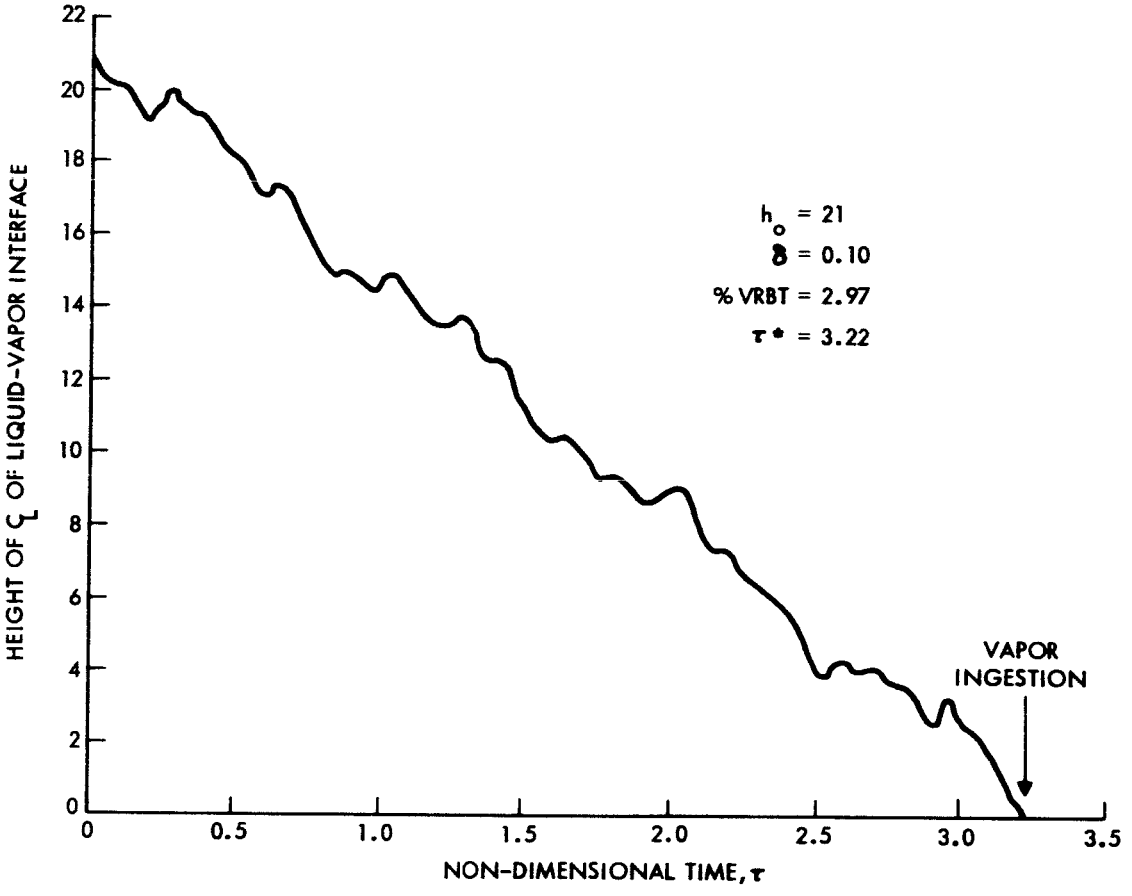

FIGURE 7. — Time-History of Position of Centerline of Liquid-Vapor Interface During Draining at We = 10

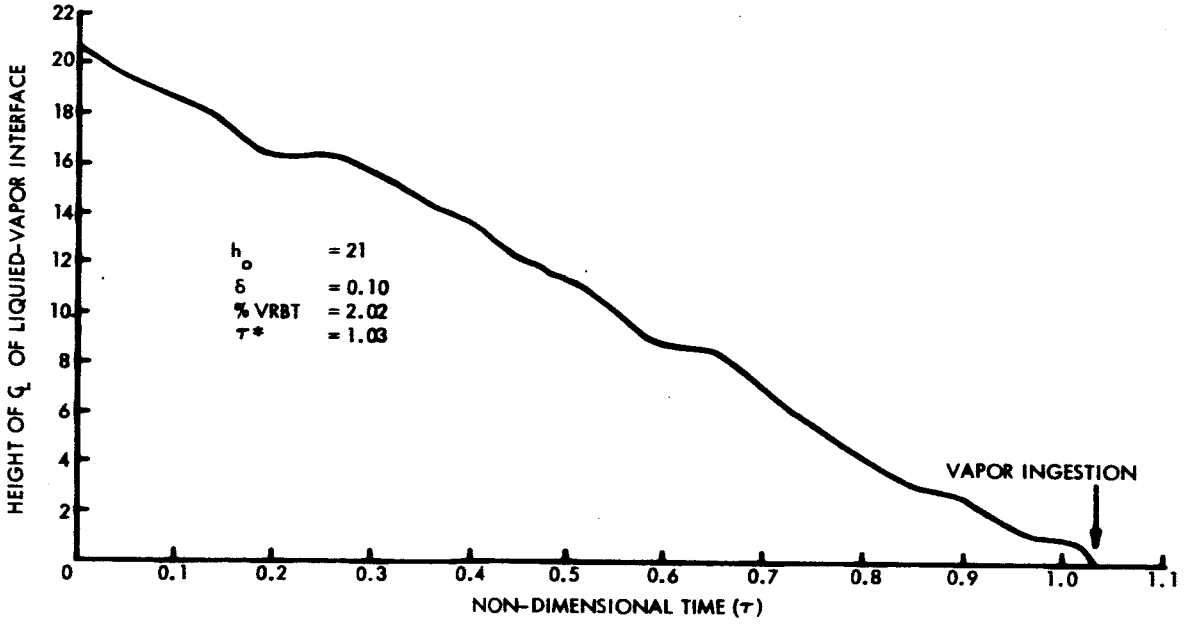

FIGURE 8. — Time-History of Position of Centerline of Liquid-Vapor Interface During Draining at We = 100

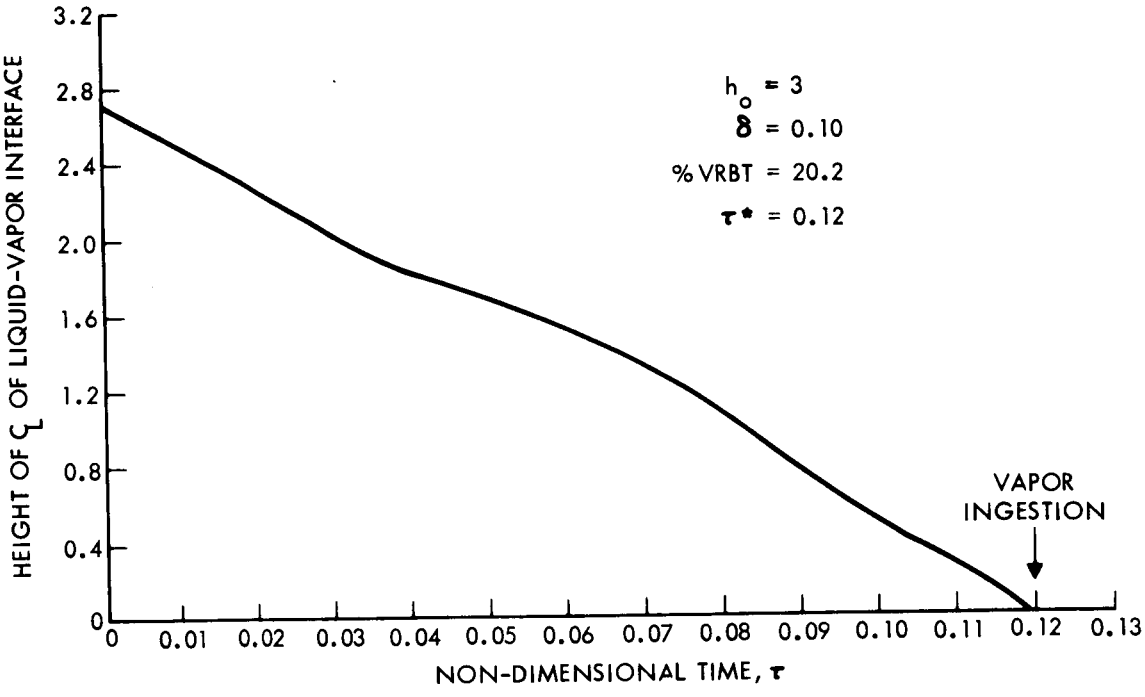

FIGURE 9. — Time-History of Position of Centerline of Liquid-Vapor Interface During Draining at We = 100

took place in Figure 9 was about 1/7 of the fundamental sloshing period. Very little free surface oscillations are present. Figure 10 illustrates the case of We = 10 with h_o = 3. The blowthrough time is about one-half of the period of the fundamental slosh mode. For h_o = 3, a Weber number of 0.2 corresponds to about 3 cycles of the fundamental period, We = 0.4 to about 2.5 cycles, We = 1 to about 1.7 cycles, and We = 3 to about 1 cycle. This is discussed in more detail in the next section.

In view of this, it is apparent that, in the absence of any dissipative mechanism, there will be appreciable oscillations of the free surface as the liquid drains from the tank. Only for a very high draining rate will there be a negligible amount of free surface oscillation. This is illustrated in Figures 11 and 12. Figure 11 shows the shape of the free surface at different times until vapor ingestion occurs. The curve at $\tau = 0$ also compares the result of truncating the series at 6 terms with the initial hemispherical shape. The representation of the initial shape is seen to be adequate for the purposes of this study. Figure 12 shows the corresponding time history of the position of the centerline of the free surface.

Since the series, Equation (33), must be truncated at a finite number of terms, it is of interest to examine how the results are affected by the number of terms. An indication of this is presented in Table I in which the percent volume of liquid remaining (%VRBT) and the time for vapor ingestion are given for truncation of the series at different terms. In the numerical work, six terms were nominally used, and Table I is evidence that this has provided adequate accuracy.

TABLE I. —Effect of Truncation of Series in Equation (33) at Different Numbers of Terms

$h_o = 3$, $\frac{\sigma}{\rho} = 30\ cm^3/sec^2$, $\delta = 0.10$, We = 0.2			
No. of Terms	4	6	10
%VRBT	25.81	25.75	25.72
τ^*	2.489	2.491	2.493

(a)

$h_o = 3$, $\frac{\sigma}{\rho} = 28.5\ cm^3/sec^2$, $\delta = 0.10$, We = 3.6							
No. of Terms	1	2	3	4	5	6	9
%VRBT	16.31	14.61	13.59	13.76	13.73	13.89	13.81
τ^*	0.663	0.677	0.685	0.683	0.683	0.682	0.683

(b)

Tables II, III, IV, and V give the results for the cases listed in Section 7. Inspection of the tables fails to reveal any significant trend to the value of %VRBT as related to We.

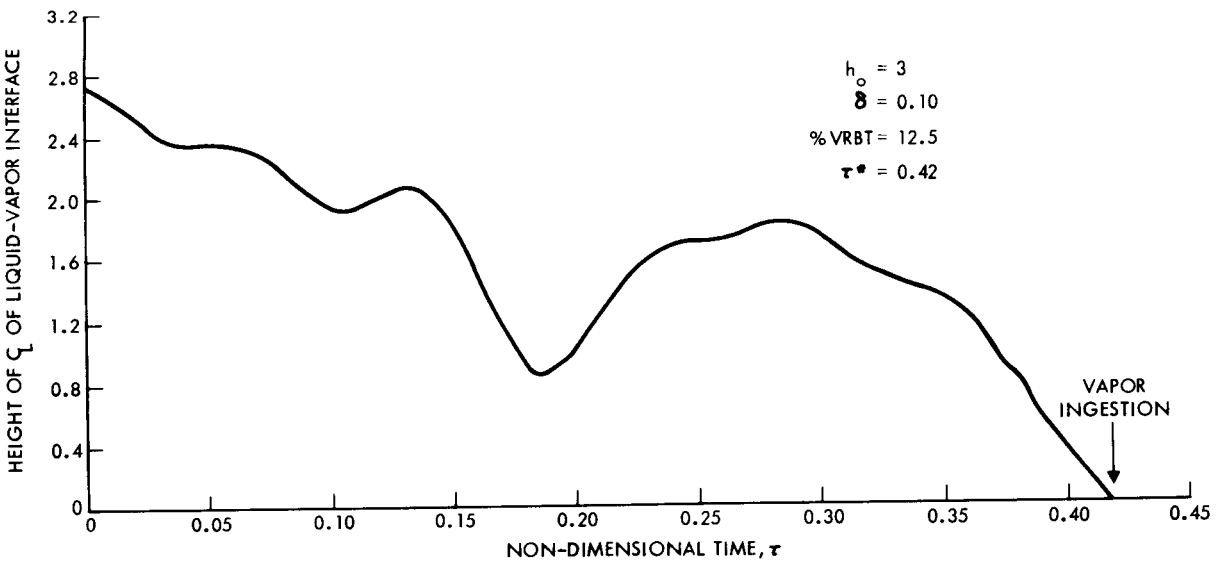

FIGURE 10. —Time-History of Position of Centerline of Liquid-Vapor Interface During Draining at We = 10

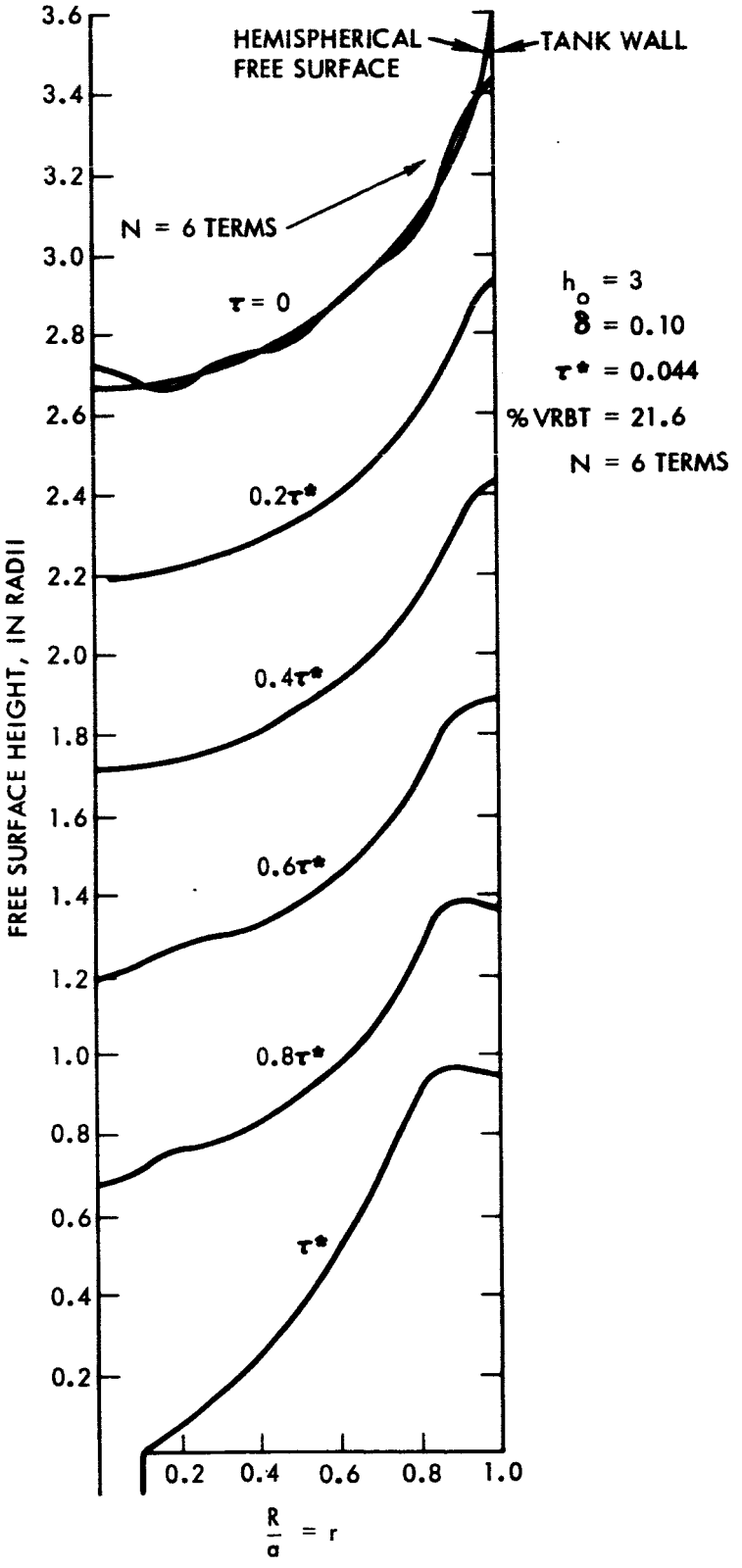

FIGURE 11. —Typical Free Surface Distortion During Draining for We = 700

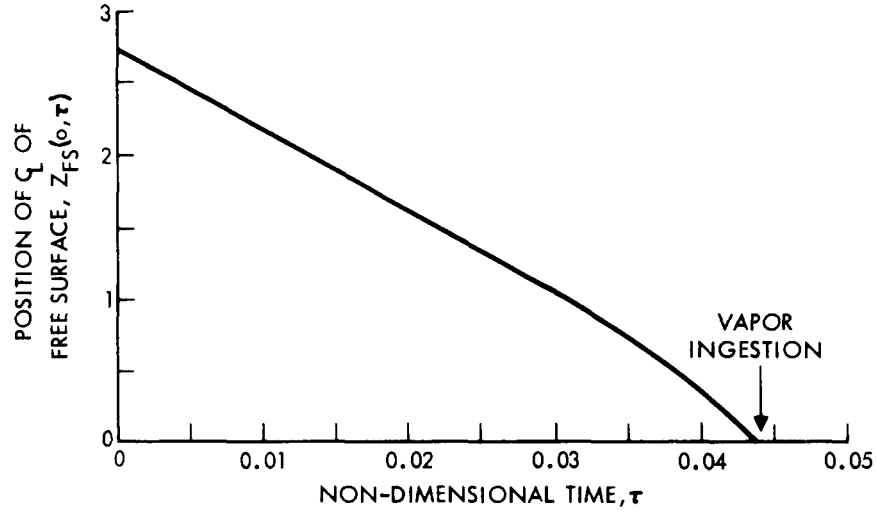

FIGURE 12. — Time-History of Position of Centerline of Free Surface. We = 700, h_o = 3, δ = 0.10, %VRBT = 21.60, τ^* = 0.044, σ/ρ = 28.4

Table II gives %VRBT and τ^* for two different initial fill levels. The results appear to be somewhat sensitive to different values of h_o, but it is difficult to deduce trends. This is so because of the oscillation of the free surface about the mean free surface as the tank drains. Depending on the initial fill level, the free surface will intersect the outlet at different phases of the cycle. If the central region of the surface has a downward velocity as it nears the outlet, then vapor ingestion will occur earlier than it would if the free surface had an upward velocity at this time. In this situation, more liquid would be left in the tank in the former case than in the latter case. This is further demonstrated in Table III.

TABLE II. —Results for Group I; $\delta = 0.10$, $\frac{\sigma}{\rho} = 30\ cm^3/sec^2$

	$h_o = 3$		$h_o = 6$	
We	%VRBT	τ^*	%VRBT	τ^*
0.2	25.75	2.49	30.56	6.50
0.4	9.89	2.14	11.61	4.19
1.0	9.36	1.36	16.36	2.51
3	16.92	0.72	11.68	1.53
10	12.46	0.42	14.22	0.81
100	20.21	0.12	6.41	0.28

TABLE III. —Variation of %VRBT and τ^* with Different Initial Fill Depths

	We = 0.2, δ = 0.10			
h_o	2	3	4	6
%VRBT	30.2	25.8	9.3	30.6
τ^*	1.56	2.49	4.06	6.50

(a)

	We = 10, δ = 0.10				
h_o	2	3	4	5	6
%VRBT	21.5	12.5	12.9	10.1	14.2
τ^*	0.25	0.42	0.55	0.71	0.81

(b)

In Table IV are presented the results for different outlet diameters. Again, it is difficult to discern trends. The results appear to be somewhat sensitive to the value of δ. This is true because of the presence of oscillations of the free surface during draining. Depending on the size of the outlet, the free surface may contact the edge of the outlet during one, or may not intersect until the next, cycle. This effect of outlet diameter is especially critical depending on whether the oscillation of the centerline of the free surface about the mean free surface is on a downward or an upward cycle at the time the free surface is near the edge of the outlet diameter. In addition, the larger outlet has an inherent tendency to delay vapor ingestion because the curved free surface would have to drop lower to contact the outlet. This is illustrated in Figure 13.

TABLE IV. —Effect of Outlet Diameters

	Results for Group II; $h_o = 3$, $\frac{\sigma}{\rho} = 30\ cm^3/sec^2$					
	$\delta = 0.05$		$\delta = 0.10$		$\delta = 0.20$	
We	%VRBT	τ^*	%VRBT	τ^*	%VRBT	τ^*
0.2	25.84	2.49	25.75	2.49	6.58	3.14
1	10.39	1.34	9.36	1.36	8.49	1.37
3	16.74	0.72	16.92	0.72	16.72	0.72
10	12.60	0.41	12.46	0.42	11.81	0.42

	Results for Group III; $h_o = 3$, $\frac{\sigma}{\rho} = 70\ cm^3/sec^2$			
	$\delta = 0.10$		$\delta = 0.20$	
We	%VRBT	τ^*	%VRBT	τ^*
0.2	25.75	2.49	6.59	3.14
1	9.36	1.36	8.49	1.37
3	16.92	0.72	16.91	0.72
10	12.46	0.42	11.81	0.42

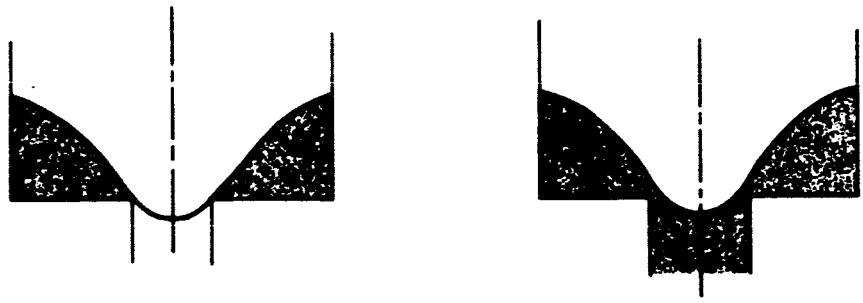

(a) SMALLER OUTLET, EARLIER VAPOR INGESTION, LARGER %VRBT

(b) LARGER OUTLET, VAPOR INGESTION DELAYED, SMALLER %VRBT

FIGURE 13. —Effect of Outlet Diameter

The effect of varying σ/ρ is shown in Table V. The non-dimensional results appear to be independent of the value of σ/ρ. This follows from the fact that the non-dimensionalization has removed σ/ρ as a separate parameter of the problem. Thus, the non-dimensionalized equations are independent of σ/ρ. The corresponding dimensional results will, of course, reflect changes in this quantity.

TABLE V. —Effect of Different Values of $\frac{\sigma}{\rho}$ for $h_o = 3$, $\delta = 0.10$

	$\frac{\sigma}{\rho} = 10\ cm^3/sec^2$		$\frac{\sigma}{\rho} = 30\ cm^3/sec^2$		$\frac{\sigma}{\rho} = 70\ cm^3/sec^2$	
We	%VRBT	τ^*	%VRBT	τ^*	%VRBT	τ^*
0.2	25.75	2.49	25.75	2.49	25.75	2.49
1	9.36	1.36	9.36	1.36	9.36	1.36
3	16.92	0.72	16.92	0.72	16.92	0.72
10	12.46	0.42	12.46	0.42	12.46	0.42

10. EFFECT OF OSCILLATIONS ON THE DRAINING PROCESS

In the previous section, the oscillations of the free surface during draining were discussed. There will always be the presence of oscillations, but whether or not they will appreciably affect the draining process depends on the draining rate and the initial fill level. In general, the faster draining rates (large Weber

number) and lower fill levels are associated with fewer oscillations, and the slower draining rates (small Weber number) and larger fill levels are associated with many oscillations.

The question arises, then, as to how to determine, a priori, whether or not the designer need be concerned with the oscillations. From Equation (36), in the absence of gravity, the period of fundamental mode of oscillation may be approximated as

$$\tau_f = \frac{2\pi}{\omega_f} = \frac{2\pi}{\gamma_1^{3/2}\sqrt{\tanh \gamma_1 h}} \tag{48}$$

where γ_1 is the first root of $J_1(\gamma_n) = 0$, i.e., $\gamma_1 = 3.83$. Since $\tanh x = 1$ for $x > 2$, the factor

$$\tanh \gamma_1 h$$

is virtually unity except when $h < 0.5$. Hence, for present purposes, we can set $\tanh \gamma_1 h = 1$ in Equation (48) and get

$$\tau_f = \frac{2\pi}{\gamma_1^{3/2}} \tag{49}$$

An estimate of the draining time can be obtained from

$$\tau^*_{est} = \frac{ho}{\alpha} = \frac{ho}{2\sqrt{We}} \tag{50}$$

From Equations (49) and (50), an estimate of the number of oscillations of the liquid-vapor interface can be obtained from

$$\frac{\tau^*_{est}}{t_f} = \frac{h_o \gamma_1^{3/2}}{4\pi\sqrt{We}} = 0.59 \frac{h_o}{\sqrt{We}} \tag{51}$$

If this number is small, then there are few oscillations during outflow; a large number represents many oscillations. The designer must determine the importance of the oscillations for the particular application involved. While many oscillations may introduce difficulties in some cases, it should be remembered that at low fillings even one oscillation can greatly affect %VRBT and τ^* depending

on whether the interface is on an upward or downward cycle at the time of vapor ingestion.

11. EFFECT OF VISCOSITY

In the foregoing analysis the viscosity of the liquid has been neglected. In any physical problem, the liquid will have some viscosity, although for many situations its effects may be small and can be neglected outside the boundary layer. It is of some interest, then, to estimate the thickness of the boundary layer to check if our results are consistent with the inviscid assumption. If the thickness is small in comparison with the radius of the container, then it is reasonable to neglect viscosity and treat the liquid as inviscid. If the boundary layer thickness is appreciable, then the assumption of an inviscid liquid is not appropriate and the results obtained in this study may not apply for certain cases (as in small sized tanks).

The thickness δ^* of the boundary layer can be estimated from[†]

$$\frac{\delta^*}{L} = \frac{5}{\sqrt{Re}} \tag{52}$$

where L is a characteristic length, Re is Reynolds number given by $Re = UL/\nu$ U is a characteristic velocity, and ν the kinematic viscosity.

For purposes of illustration, a representative case from the experimental work described in Reference 5 is considered. For this case,

$$\begin{aligned} U &= 14.27 \text{ cm/sec} = \text{velocity of mean free surface} \\ a &= 2 \text{ cm.} = \text{radius of container} \\ \nu &= 0.0152 \text{ cm}^2/\text{sec} \\ L &= 6 \text{ cm} = \text{liquid depth} \end{aligned} \tag{53}$$

These numbers correspond to a typical drop test conducted at NASA Lewis Research Center and are discussed in Reference 5. Corresponding to (49),

$$Re = \frac{UL}{\nu} \approx 5630 \tag{54}$$

and

$$\delta^* = 0.067L = 0.40 \text{ cm}$$

[†]Reference 4, p. 24, Equation (2.2). This is Blasius' formula for the flow of a viscous fluid over a flat plate.

Actually, the boundary layer thickness builds up from zero to the maximum of 0.40 cm, so that an average value of the boundary layer in this test could be taken as 0.20 cm. This is appreciable when compared with the container radius of 2 cm and suggests that the effects of viscosity may be important in a container this small. For a large tank, the effects of viscosity would be less significant because the ratio of the boundary layer thickness to the tank radius would be small. It may be remarked that in the above method of estimating the thickness of the boundary layer, the thickness is independent of the tank radius.

Equation (52) was based on steady flow considerations, whereas the draining problem is a transient one. Another estimate of the boundary layer thickness can be found from†

$$\delta^* = 4\sqrt{\nu t} \tag{55}$$

which is based on the theoretical solution for a suddenly accelerated plane wall. The value for t can be taken as the time to vapor ingestion. For the case of Equation (55),

$$t = \frac{L}{U} = \frac{6}{14.27} = 0.42 \text{ sec} \tag{56}$$

Then

$$\delta^* = 4\sqrt{0.0152(0.42)} = 4(0.0064) = 0.32 \text{ cm} \tag{57}$$

Hence, the above conclusions concerning viscosity appear to be valid. Both methods of estimating the boundary layer thickness give results which are of the same order of magnitude. These estimates indicate a boundary layer thickness ranging from 10 to 16% of the tank radius for the numerical example considered in this section.

12. SUMMARY AND CONCLUSIONS

The results obtained in this study can be summarized as follows:

(1) A linearized solution to the problem of draining a liquid from a container in a zero-g environment has been formulated and numerical cases examined.

(2) Scaling laws have been derived. For dynamical similarity between two draining problems, one must maintain the values of Weber number, initial fill depth to tank radius ratio, and outlet radius to tank radius ratio.†† The times are then relatable through Equation (46).

† Reference 4, p. 65

†† Bond number must also be preserved if the draining is under conditions of low gravity rather than in a state of complete weightlessness.

(3) As the liquid drains from the tank, the free surface oscillates about its downward-moving mean position.

(4) For slow draining rates (corresponding to small values of Weber number), there may be many oscillations of the liquid-vapor interface before vapor ingestion ends the draining process.

(5) The %VRBT and the time for vapor ingestion appear to be sensitive to outlet diameter and to the initial fill level because of the free surface oscillations during draining. Depending on whether or not the center-line of the free surface is moving down or up at the time when the free surface is near the outlet, then blowthrough will be accelerated or delayed and the value of %VRBT will be larger or smaller.

(6) Further, the larger outlet diameter has the inherent tendency to delay vapor ingestion (because the mean free surface must drop lower), thereby permitting more complete drainage from the tank.

(7) Because of the nature of the non-dimensionalization employed, the numerically given results are independent of the tank radius and the ratio σ/ρ. The dimensional quantities, of course, reflect these parameters.

(8) The effect of viscosity on the draining process is generally small and has been neglected in the analysis. However, if the tank has a very small radius, then the effects of viscosity may become important.

(9) A criterion has been developed to assist the designer in determining whether or not the oscillations during the draining process will be important in a particular case of interest.

The above results have been obtained from a linear analysis and demonstrate all of the significant features of the phenomenon that have been experimentally observed. There are limitations, however, in the linear theory employed. Should it be desirable to remove these limitations, then a nonlinear analysis would be in order. It might also be possible to include, in an approximate manner, the effects of viscosity so that a more detailed comparison of theory with experiment might be obtained.

REFERENCES

1. P. G. Bhuta and L. R. Koval, "Sloshing of a Liquid in a Draining or Filling Tank Under Variable G Conditions," Symposium on Fluid Mechanics and Heat Transfer Under Low Gravitational Conditions, Sponsored by the United States AFOSR and Lockheed Missiles and Space Co., 24-25 June 1965, Palo Alto, California.

2. H. Lamb, Hydrodynamics, 6th Edition, Chapter IX, Dover Publications, New York, 1945, p. 364.

3. N. W. McLachlan, Bessel Functions for Engineers, Oxford University Press, London, Second Edition, 1955.

4. H. Schlichting, Boundary Layer Theory, Pergamon Press, New York, 1955.

5. R. C. Nussle, J. D. Derdul, and D. A. Petrash, "Photographic Study of Propellant Outflow from a Cylindrical Tank During Weightlessness," NASA TN D-2572, January, 1965.

ACKNOWLEDGEMENT

The authors wish to thank Donald Petrash and Lynn Grubb of NASA Lewis Research Center for the interesting and helpful discussions during this study.

APPENDIX A
PARABOLIC OUTLET VELOCITY

In this appendix, the analysis of reference 1 is extended to the case of parabolic velocity distribution at the tank outlet.

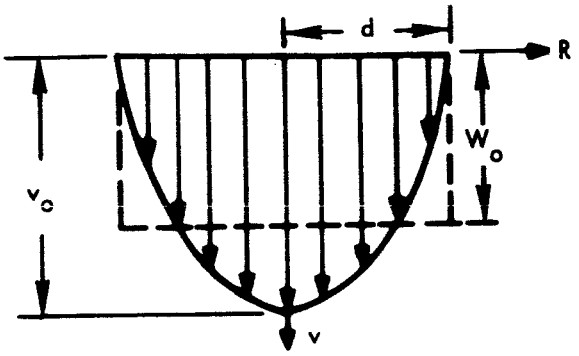

FIGURE 14. —Outlet Velocity Profile

The variation in the velocity is given by

$$v(R) = v_o\left(1 - \frac{R^2}{d^2}\right), \quad 0 \leq R \leq d$$

$$= 0 \qquad\qquad , \quad d \leq R \leq a \tag{A1}$$

In terms of an average outlet velocity, W_o,

$$v(R) = 2W_o\left(1 - \frac{R^2}{d^2}\right), \quad 0 \leq R \leq d$$

$$= 0 \qquad\qquad , \quad d \leq R \leq a \tag{A2}$$

Equation (17) requires that

$$\left.\frac{\partial \phi}{\partial Z}\right|_{Z=0} = \begin{cases} -2W_o\left(1 - \frac{R^2}{d^2}\right), & 0 \leq R \leq d \\ 0 \qquad\qquad , & d \leq R \leq a \end{cases} \tag{A3}$$

and we wish to expand the right hand side of Equation (A3) in a Fourier-Bessel series of $J_o(k_n R)$. Accordingly,

$$v(R) = A_o + \sum_{n=1}^{\infty} A_n J_o(k_n R) \tag{A4}$$

where

$$A_o = \frac{2}{a^2} \int_o^a R\left\{2W_o f(t)\left[1 - \frac{R^2}{d^2}\right]\right\} dR = \frac{W_o f(t) d^2}{a^2} \tag{A5}$$

and

$$A_n = \frac{1}{C_n} \int_o^d R\left\{2W_o f(t)\left[1 - \frac{R^2}{d^2}\right]\right\} J_o(k_n R)\, dR \tag{A6}$$

where

$$C_n = \int_o^a J_o^{\,2}(k_n R)\, RdR = \frac{a^2}{2} J_o^{\,2}(k_n a) \tag{A7}$$

The integral in Equation (A6) can be evaluated from the integral

$$\int_o^d \left(1 - \frac{Z^2}{a^2}\right)^{n+1} J_o(kZ)\, ZdZ = \frac{2^{n+1}(n+1)!\; d^2}{(kd)^{n+2}} J_{n+2}(kd) \tag{A8}$$

which is given in McLachlan, Reference 3, page 63. Picking n = 0,

$$\int_o^d \left(1 - \frac{Z^2}{a^2}\right) J_o(kZ)\, ZdZ = \frac{2}{k^2} J_2(kd) \tag{A9}$$

Combining Equations (A6), (A7), and (A9),

$$A_n = \frac{8W_o f(t)}{(k_n a)^2} \frac{J_n(k_n d)}{J_o^{\,2}(k_n a)} \tag{A10}$$

where

$$J_2(k_n d) = \frac{2}{k_n d} J_1(k_n d) - J_o(k_n d) \tag{A11}$$

Finally, the expansion of the outlet velocity is

$$v(R) = \frac{W_o d^2 f(t)}{a^2} + 8W_o f(t) \sum_{n=1}^{\infty} \frac{J_2(k_n d)\, J_o(k_n R)}{(k_n a)^2 J_o^2(k_n a)} \tag{A12}$$

and Equation (18) in the text follows.

APPENDIX B

EXPANSION OF INITIAL FREE SURFACE CONFIGURATION

In this section, the analysis of reference 1 is extended to consider the hemispherical quiescent free surface at the inception of draining.

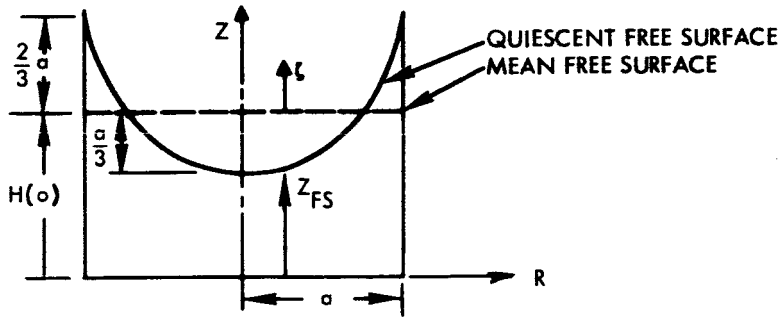

FIGURE 15. —Geometry of Initial Free Surface

In a weightless environment, the quiescent free surface may be approximated by a hemispherical shape given by

$$Z_{FS}(R) = H(0) + \frac{2}{3}a - \sqrt{a^2 - R^2} \tag{B1}$$

Writing

$$Z_{FS}(R) = H(0) + \zeta(R, o) \tag{B2}$$

then

$$\zeta(R, 0) = \frac{2}{3}a - \sqrt{a^2 - R^2} \tag{B3}$$

describes the initial shape of quiescent free surface. Expanding Equation (B3) in a Fourier-Bessel series,

$$\zeta(R, 0) = \sum_{n=1}^{\infty} C_{no} J_o(k_n R) \tag{B4}$$

the coefficient, C_{no}, is given by

$$C_{no} = \frac{\int_o^a \left(\frac{2}{3}a - \sqrt{a^2 - R^2}\right) J_o(k_n R)\, RdR}{\int_o^a J_o^2(k_n R)\, RdR} \tag{B5}$$

The integral in the denominator of equation (B5) is

$$\int_o^a J_o^2(k_n R)\, RdR = \frac{a^2}{2} J_o^2(k_n a) \tag{B6}$$

The numerator includes the integral

$$\int_o^a J_o(k_n R)\, RdR = \frac{a}{k_n} J_o(k_n a) \tag{B7}$$

and the integral

$$I = \int_o^a \sqrt{a^2 - R^2}\, J_o(k_n R)\, RdR \tag{B8}$$

To evaluate Equation (B8), let $R = a \sin\theta$. Upon substitution into Equation (B8),

$$I = a^3 \int_o^{\pi/2} J_o(k_n a \sin\theta) \sin\theta \cos^2\theta\, d\theta \tag{B9}$$

From McLachlan, Reference 3, page 194, Equation (63).

$$\int_0^{\pi/2} J_o(Z \sin\theta) \sin^{\nu+1}\theta \cos^{2\mu+1}\theta = \frac{2^{\mu}\Gamma(\mu+1)}{Z^{\mu+1}} J_{\mu+\nu+1}(Z) \qquad \text{(B10)}$$

where $\Gamma(x)$ is the gamma function. Letting $\nu = 0$, $\mu = 1/2$, $z = k_n a$ in Equation (B10) yields

$$\int_0^{\pi/2} J_o(Z \sin\theta) \sin\theta \cos^2\theta \, d\theta = \frac{\sqrt{2}\,\Gamma(3/2)}{(k_n a)^{3/2}} J_{3/2}(k_n a) \qquad \text{(B11)}$$

Then

$$I = a^3 \frac{\sqrt{2}\,\Gamma(3/2)}{(k_n a)^{3/2}} J_{3/2}(k_n a) \qquad \text{(B12)}$$

Combining Equations (B5), (B6), (B7), and (B8), yields

$$C_{no} = -\frac{2\sqrt{2}\, a\,\Gamma(3/2)\, J_{3/2}(k_n a)}{(k_n a)^{3/2}\, J_o^{\,2}(k_n a)} \qquad \text{(B13)}$$

Introducing the nondimensional terms from Equation (32), Equation (13) takes the form

$$\zeta_{no} = -\frac{2\sqrt{2}\,\Gamma(3/2)\, J_{3/2}(\gamma_n)}{\gamma_n^{3/2}\, J_o^{\,2}(\gamma_n)} \qquad \text{(B14)}$$

where γ_n are the roots of $J_1(\gamma_n) = 0$.

NOMENCLATURE

a	Outer radius of tank
A	Constant velocity of mean free surface (draining rate)
$\dot{A}_o(t)$	Function of time, Equation (14)
$\dot{A}_n(t)$	Function of time, Equation (13)
$\dot{B}_o(t)$	Function of time, Equation (14)
$\dot{B}_n(t)$	Function of time, Equation (13)
B_o	Bond number = $\rho g a^2/\sigma$
$C_n(t)$	Generalized coordinate for free surface distortion, Equation (16)
d	Outlet radius
$f(t)$	Time variation of outlet velocity
g	Gravitational acceleration
$H(t)$	Mean free surface height
$h(\tau)$	Nondimensional mean free surface height
h_o	Initial value of $h(\tau)$
J_m	Bessel function of first kind and order m
k_n	Separation constant for Laplace's equation
p	Pressure
r	Nondimensional radial coordinate
(R, θ, Z)	Dimensional cylindrical coordinates
Re	Reynolds number = inertial forces/viscous forces
t	Time
u, v, w	Components of liquid velocity
U	Characteristic velocity, Equation (47)
V_{BT}	Volume liquid remaining in tank at blowthrough (vapor ingestion)

NOMENCLATURE (Concluded)

W_o	Average outlet velocity
We	Weber number = inertial forces/surface tension forces
$z = \frac{Z}{a}$	Nondimensional vertical coordinate
Z_{FS}	Vertical coordinate of free surface
$\alpha = A\sqrt{\frac{\rho a}{\sigma}}$	Nondimensional draining rate
Γ	Gamma function
$\gamma_n = k_n a$	Root of $J_1(\gamma_n) = 0$
$\delta = d/a$	Nondimensional outlet radius
δ^*	Thickness of boundary layer
ζ	Free surface displacement from the mean free surface
ν	Kinematic viscosity
ξ	Nondimensional generalized coordinate
ρ	Liquid density
σ	Surface tension
τ	Nondimensional time
τ^*	Nondimensional time for vapor ingestion
τ_f	Period of fundamental slosh mode
ϕ	Velocity potential
% VRBT	Percentage volume of liquid remaining in tank at blowthrough

REPORT DISTRIBUTION LIST FOR
CONTRACT NAS 3-7931

MANDATORY

Recipient/No. of Copies	Address
1. NASA Headquarters FOB-10B Attn: RV-1/Warren Keller (1)	NASA Headquarters 600 Independence Avenue S. W. Washington, D. C. 20546
2. NASA Lewis Research Center Attn: Spacecraft Technology Procurement Section (M. S. 54-2) (1) Attn: Technology Utilization Office (M. S. 3-19) (1) Attn: Technical Information Division (M. S. 5-5) (1) Attn: Library (M. S. 60-3) (2) Attn: Spacecraft Technology Division (M. S. 54-1) a. C. C. Conger (2) b. D. A. Petrash (20) Attn: Report Control Office (M. S. 5-5) (1)	NASA Lewis Research Center 21000 Brookpark Road Cleveland, Ohio 44135
3. NASA Scientific and Technical Information Facility Attn: NASA Representative RQT-2448 (6)	NASA Scientific and Technical Information Facility P. O. Box 33 College Park, Maryland 20740
4. Research and Technology Division Wright-Patterson AFB Attn: AFAPL (APIE-2)/ R. F. Cooper (1)	Wright-Patterson AFB, Dayton, Ohio 45433
5. AFWL Kirtland AFB Attn: WLPC/Capt. C. F. Ellis (1)	AFWL Kirtland AFB New Mexico
6. Aerospace Corporation Attn: Library/Technical Documents Group (1)	Aerospace Corporation P. O. Box 95085 Los Angeles, California 90045
7. Westinghouse Astronuclear Laboratories Attn: H. W. Szymanowski (1)	Westinghouse Astronuclear Laboratories Electric Propulsion Laboratory Pittsburgh, Pennsylvania 15234